

Limits on the cosmic-ray ionization rate toward massive young stars

Floris F.S. van der Tak and Ewine F. van Dishoeck

Sterrewacht, Postbus 9513, 2300 RA Leiden, The Netherlands

Received May 5, 2000 / Accepted May 27, 2000

Abstract. Recent models of the envelopes of seven massive protostars are used to analyze observations of H_3^+ infrared absorption and H^{13}CO^+ submillimeter emission lines toward these stars, and to constrain the cosmic-ray ionization rate ζ_{CR} . The H^{13}CO^+ gives best-fit values of $\zeta_{\text{CR}} = (2.6 \pm 1.8) \times 10^{-17} \text{ s}^{-1}$, in good agreement with diffuse cloud models and with recent Voyager/Pioneer data but factors of up to 7 lower than found from the H_3^+ data. No relation of ζ_{CR} with luminosity or total column density is found, so that local (X-ray) ionization and shielding against cosmic rays appear unimportant for these sources. The difference between the H_3^+ and H^{13}CO^+ results and the correlation of $N(\text{H}_3^+)$ with heliocentric distance suggest that intervening clouds contribute significantly to the H_3^+ absorptions in the more distant regions. The most likely absorbers are low-density ($\lesssim 10^4 \text{ cm}^{-3}$) clouds with most carbon in neutral form or in CO.

Key words: ISM: Cosmic rays – Molecules – Structure

1. Introduction

The ionization fraction of molecular clouds is an important parameter for their dynamics through its control over the influence of any magnetic field. The ionization also has a major effect on the chemistry of molecular clouds because ion-neutral reactions are generally much faster than neutral-neutral reactions. In dense regions shielded from direct ultraviolet irradiation, the ionization is dominated by cosmic rays. However, the rate of this process ζ_{CR} has not yet been constrained directly. The current best estimate comes from chemical models to reproduce the observed abundances of OH and HD in diffuse interstellar clouds (Hartquist et al. 1978; van Dishoeck & Black 1986; Federman et al. 1996), notably those toward Perseus OB2. These models indicate that $\zeta_{\text{CR}} = 10^{-16} - 10^{-17} \text{ s}^{-1}$ per H atom, but with a factor of 10 uncertainty because of uncertainties in temperature, radiation field and the effects

of shocks. In addition, it is unknown if ζ_{CR} varies with location in the Galaxy, since the diffuse cloud results are limited to the solar neighbourhood.

Each cosmic-ray ionization of H_2 yields one H_3^+ molecule, so that H_3^+ has a constant concentration which depends only on ζ_{CR} and the abundances of its main destroyers: CO, O and electrons. Hence, the recent detections of H_3^+ infrared absorption lines by Geballe & Oka (1996) and McCall et al. (1999) toward massive protostars provide a novel way to measure ζ_{CR} . We constrain ζ_{CR} using models by van der Tak et al. (2000) of the envelopes of these stars, and use the derived values to model observations of HCO^+ , the abundance of which is also proportional to ζ_{CR} .

2. Models

McCall et al. (1999) present observations of rovibrational lines of H_3^+ in absorption against seven luminous ($10^4 - 10^5 L_{\odot}$) young stars, which are still embedded in envelopes of $\sim 100 M_{\odot}$ of dust and molecular gas. These same sources have been studied by Mitchell et al. (1990) in ^{13}CO infrared absorption and by van der Tak et al. (2000) in submillimeter dust continuum and CS, C^{34}S and C^{17}O line emission. Based on these data sets, van der Tak et al. (1999, 2000) modeled the temperature and density structure of the envelopes using a power law structure $n = n_0(r/r_0)^{-\alpha}$. The radial dust temperature profile is calculated self-consistently from the luminosity and n_0 is determined from submillimeter photometry which probes the dust column density. The parameter α is constrained by modeling the relative strengths of the CS and C^{34}S $J = 2 \rightarrow 1$ through $10 \rightarrow 9$ lines with a non-LTE radiative transfer program based on the Monte Carlo method.

The outer radii of the models are twice the half-intensity radii of the CS $J = 5 \rightarrow 4$ emission, given in Table 5 of van der Tak et al. (2000). For the sources studied here, the values are $(3 - 11) \times 10^{17} \text{ cm}$, which are accurate to a factor of 2. However, the dust and gas maps also reveal emission extending outside the envelopes of W 3

Table 1. Observed and modeled column densities and ortho/para ratios of H_3^+ and CO.

Source	Observed ^(a)			Modeled ^(b)			Inferred ζ_{CR} ^(c)	
	$N(\text{H}_3^+)$ 10^{13} cm^{-2}	o/p ratio	$N(\text{CO})$ 10^{19} cm^{-2}	$N(\text{H}_3^+)$ 10^{13} cm^{-2}	o/p ratio	$N(\text{CO})$ 10^{19} cm^{-2}	(1) 10^{-17} s^{-1}	(2)
GL 2136	38 ± 4	$1.0^{+0.4}_{-0.3}$	2.2	3.9	0.45	3.6	9.7	16
GL 2591	22 ± 2	$0.8^{+0.2}_{-0.1}$	1.3	2.0	0.46	2.1	11	18
GL 490	11 ± 6	$0.6^{+1.6}_{-0.5}$	0.78	5.2	0.19	8.4	2.1	23
W 33A	52 ± 13	$0.8^{+0.5}_{-0.3}$	2.6	16.6	0.26	7.8	3.1	9.3
NGC 2264	< 12	–	2.2	3.1	0.29	7.2	< 3.9	< 13
W3 IRS5	< 8.6	–	2.6	4.3	0.51	9.4	< 2.0	< 7.2
S 140	< 4.4	–	0.74	2.3	0.41	6.3	< 1.9	< 16

^a H_3^+ from McCall et al. (1999); CO from ^{13}CO observations by Mitchell et al. (1990, 1993, 1995).

^b Using the physical structure from van der Tak et al. (2000) and assuming $\zeta_{\text{CR}} = 1 \times 10^{-17} \text{ s}^{-1}$.

^c Case (1): $(N_{\text{obs}}(\text{H}_3^+) / N_{\text{model}}(\text{H}_3^+)) \times 10^{-17} \text{ s}^{-1}$; case (2) = case (1) $\times (N_{\text{obs}}(\text{CO}) / N_{\text{model}}(\text{CO}))$.

IRS5 and GL 490, and maybe W 33A. No “skin” appears to surround GL 2591 and GL 2136. The case of S 140 is complicated: the dust appears to be heated by multiple sources, and its emission is not well fitted by a centrally heated model. We do not have a dust map of NGC 2264, but this source is part of an extended molecular cloud complex, so that extended material may also contribute to the H_3^+ absorption. Evidence for extended components at lower temperature and/or column density than those probed by the dust emission comes from emission in low- J lines of CO at $\gtrsim 1'$ offsets, and self-absorptions on their central line profiles. These features are present in the data for all the sources discussed in this paper. Before considering foreground contributions in § 5, we concentrate on the dense molecular envelopes.

3. Results

Given the temperature and density profiles, we calculate the H_3^+ concentration at each position in the envelopes. Considering only cosmic rays as producers of H_3^+ and reactions with CO and O as destroyers, the concentration of H_3^+ is given by $n(\text{H}_3^+) = \zeta_{\text{CR}} / [x(\text{CO}) \times k_{\text{CO}} + x(\text{O}) \times k_{\text{O}}]$. In this expression, $x(\text{CO})$ and $x(\text{O})$ are the abundances of CO and O relative to H_2 , and k_{CO} and k_{O} the rate coefficients for their respective reactions with H_3^+ , taken from Millar et al. (1997). We neglect any dependence of k_{CO} on temperature since the dipole moment of CO is small. The models use an abundance of CO of 2×10^{-4} at temperatures above 20 K, and zero below due to freeze-out on dust grains. This abundance behaviour is consistent with observations of C^{17}O emission lines by van der Tak et al. (2000). The abundance of O is assumed to be 1.5×10^{-4} based on the models of Lee et al. (1996), and the temperature in our models does not drop below 14 K, where O would freeze out. The ortho/para (o/p) or $(J, K) = (1, 0)/(1, 1)$ ratio of H_3^+ changes with radius since the ground state of ortho- H_3^+ lies 32.86 K above that of para- H_3^+ (Dinelli et al. 1997), and reactive collisions with

H_2 tie the o/p ratio to the kinetic temperature. Figure 1 illustrates the results for the case of GL 2136.

Integration of the concentrations of ortho- and para- H_3^+ over radius yields total column densities $N(\text{H}_3^+)$ and mean o/p ratios, which are compared with the data in Table 1. The calculated o/p ratios are consistent with the data within the observational errors, but the model values are systematically lower than those observed. For CO, the models, which were constrained by emission data, typically overproduce absorption measurements of $N(\text{CO})$ by factors of 3, probably due to deviations from spherical geometry on small scales, consistent with several other tracers (van der Tak et al. 2000). Since the model values of $N(\text{H}_3^+)$ may be less affected because H_3^+ is more evenly distributed than CO (Fig. 1), Table 1 presents the values of ζ_{CR} both before (case 1) and after (case 2) scaling the model down by the ratio of observed to modeled $N(\text{CO})$. The uncertainty in the model is a factor of two due to the uncertain radii of the envelopes. The estimates of ζ_{CR} in case (2) are considerably larger than those in previous work (§ 1), which together with the low o/p ratios indicates that there may be an additional component of warm H_3^+ along the line of sight. We will estimate the contribution to $N(\text{H}_3^+)$ by the dense envelopes by modeling emission lines of H^{13}CO^+ which have critical densities of $\sim 10^6 \text{ cm}^{-3}$, and hence cannot arise in the foreground.

4. Comparison with HCO^+

In the dense envelopes, the main destruction route of H_3^+ is the reaction with CO into HCO^+ . The concentration of HCO^+ is given by $n(\text{HCO}^+) = x(\text{CO})n(\text{H}_3^+)k_{\text{CO}} / [(x(e)k_e + x(\text{H}_2\text{O})k_{\text{H}_2\text{O}})]$, with k_e the rate coefficient for dissociative recombination of HCO^+ . The electron fraction $x(e)$ has been calculated at each point in the envelopes with a small chemical network (cf. de Boisanger et al. 1996) based on the UMIST reaction rates (Millar et al. 1997). The main difference with the analysis of de Boisanger et al. (1996) is the use of a detailed physical structure to in-

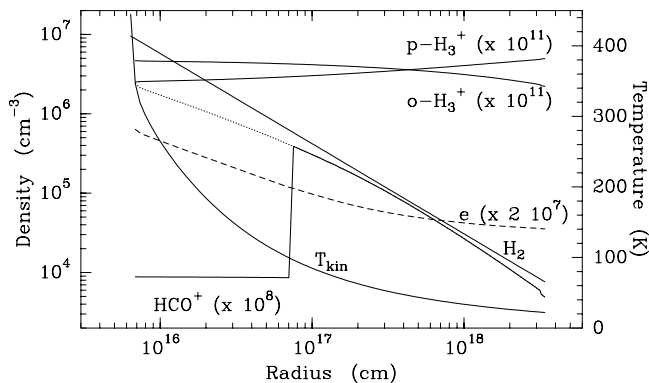
Table 2. Observed and modeled fluxes $\int T_{\text{mb}} dV$ (K km s^{-1}) of the H^{13}CO^+ $J = 3 \rightarrow 2$ and $4 \rightarrow 3$ lines.

Source	Observed		Modeled		ζ_{CR} (a)	$N(\text{H}_3^+)$ (b)
	3–2	4–3	3–2	4–3		
GL 2136	4.1	4.0	4.5	2.9	3.3	8
GL 2591	5.5	4.4	5.5	3.2	5.6	7
GL 490	2.4	1.9	3.0	2.0	0.64	0.3
W 33A	8.9	5.3	9.8	5.3	1.3	7
NGC 2264	4.0	2.1	3.3	2.4	0.61	0.6
W3 IRS5	9.3	9.2	8.2	6.0	2.8	3
S 140	9.2	8.6	8.5	6.6	3.7	1.1

(a): Best fit value of ζ_{CR} to H^{13}CO^+ data, in 10^{-17} s^{-1} .(b): Predicted from H^{13}CO^+ for case (2), in 10^{13} cm^{-2} .

interpret the high-excitation lines. We assume that O_2 and H_2O have negligible ($\lesssim 10^{-6}$) abundances in the bulk of the envelopes, but that at $T > 100$ K, $x(\text{H}_2\text{O})$ jumps to 5×10^{-5} due to grain mantle evaporation. We neglect metals such as Mg, Fe and S as contributors to $x(e)$ and large molecules such as polycyclic aromatic hydrocarbons as sinks of $x(e)$; using the low metal abundances inferred from dark cloud chemistry models would increase $x(e)$ by a factor of 2–3 (Lee et al. 1996). The values of ζ_{CR} derived above give $x(e) \sim 10^{-7}$ at the outer radii and $\sim 10^{-9}$ at the inner radii, as illustrated in Fig. 1. The precipitous drop of HCO^+ at 100 K, caused by reactions with evaporated water, occurs at too small radii to affect our results.

In the comparison with data, we use the $60\times$ less abundant isotope H^{13}CO^+ to avoid optical depth effects. The maximum optical depth in the lines is ≈ 1 in our models. Table 2 lists the calculated fluxes of the H^{13}CO^+ $J=3\rightarrow 2$ and $4\rightarrow 3$ lines in $18''$ and $14''$ beams. Observations are

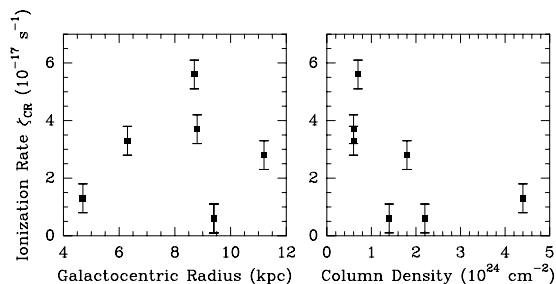
**Fig. 1.** Temperature and density structure of GL 2136, and calculated concentrations of H_3^+ , e and HCO^+ , both with (full line) and without (dotted line) destruction by H_2O included.

from van der Tak et al. (1999) for GL 2591 and from de Boisanger et al. (1996) for NGC 2264 and W 3 IRS5. The data for W 33A, GL 490, S 140 and GL 2136 were obtained with the James Clerk Maxwell Telescope in the way described in van der Tak et al. (2000). Using ζ_{CR} derived from H_3^+ , the models overproduce HCO^+ by factors of 2–7. Adjusting the models to the H^{13}CO^+ data yields refined estimates for ζ_{CR} (Table 2) which pertain strictly to the dense molecular gas, unaffected by any intervening clouds along the line of sight. The data for the various sources span the range of $\zeta_{\text{CR}} = (2.6 \pm 1.8) \times 10^{-17} \text{ s}^{-1}$, in good agreement with the diffuse cloud estimates (§ 1), and also consistent with recent data from the Voyager and Pioneer spacecraft at distances up to 60 AU from the Sun (Webber 1998).

Figure 2 shows that the source-to-source variation in ζ_{CR} is not related to Galactic structure through differences in cosmic-ray flux, nor to shielding against cosmic rays at high H_2 column densities. The values of ζ_{CR} are also unrelated to luminosity, which implies that local ionization such as by X-rays (Maloney et al. 1996) is unimportant on the scales traced by our data. Variations of the cosmic-ray density by 50% on scales of a few kpc are in good agreement with results from γ -ray observations (e.g., Hunter et al. 1997). However, why does H_3^+ give systematically higher values of ζ_{CR} ?

5. Contributions by foreground layers

Figure 3 plots the observed $N(\text{H}_3^+)$ versus heliocentric distance, including all data from McCall et al. (1999) as well as the results for the Galactic Center and the diffuse cloud in front of Cyg OB2 #12 from Geballe et al. (1999). The dense cloud data have a correlation coefficient of 93%, suggesting that absorption by intervening clouds plays an important role for the more distant sources. This section investigates the possible nature of these absorbers.

**Fig. 2.** Derived cosmic-ray ionization rates versus galactocentric radius (*left*) and $N(\text{H}_2)$ in a $15''$ beam (*right*).

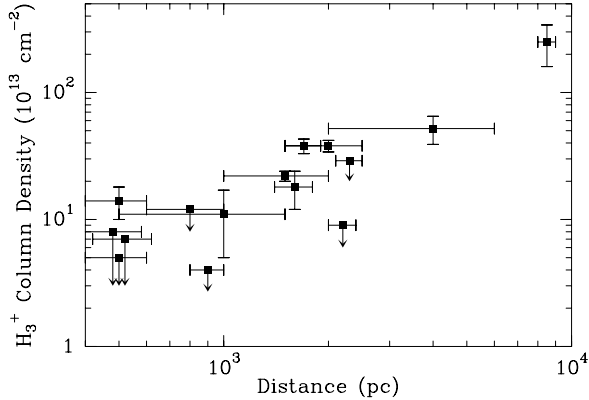


Fig. 3. Observed $N(\text{H}_3^+)$ versus heliocentric distance. The correlation suggests that intervening clouds are important.

First, the absorptions may occur at the edges of the dense cores studied here, where carbon is in neutral or ionized form. This “photodissociation region” occupies $\sim 3\text{--}4$ magnitudes of visual extinction (Hollenbach & Tielens 1997), corresponding to $N_H \lesssim 8 \times 10^{21} \text{ cm}^{-2}$. The ionized layer is negligible because the high electron fraction ($\sim 10^{-4}$) limits $n(\text{H}_3^+)$ to 10^{-7} cm^{-3} . For the neutral component, assuming $n \sim 10^4 \text{ cm}^{-3}$ as derived specifically for S 140 by Timmermann et al. (1996), and $n(\text{H}_3^+) \sim 10^{-4} \text{ cm}^{-3}$, we find $N(\text{H}_3^+) \sim \text{few} \times 10^{13} \text{ cm}^{-2}$, comparable to the dense envelopes.

Second, the absorbers may consist of cold ($\lesssim 20 \text{ K}$) molecular gas. For $n \gtrsim 10^4 \text{ cm}^{-3}$, the CO will be frozen out on the grains. Tielens et al. (1991) observed solid CO in absorption toward all our sources and found $N(\text{CO}) \sim 10^{17} \text{ cm}^{-2}$, or $N_H \sim 10^{21} \text{ cm}^{-2}$, assuming that most carbon is in solid CO. The implied column lengths are too short to be of importance for H_3^+ , and the low temperatures are incompatible with the observed $o/p \text{ H}_3^+$ ratios.

Third, the H_3^+ absorptions may arise in clouds with $n \lesssim 10^4 \text{ cm}^{-3}$, which either surround the power-law envelopes or happen to lie along the line of sight. Such “translucent” foregrounds are visible in our data (§ 2), and can contribute $N(\text{H}_3^+) \sim 10^{14} \text{ cm}^{-2}$ each based on models by van Dishoeck & Black (1989). These tenuous clouds have long path lengths and may dominate the H_3^+ absorption. At low densities, HCO^+ may form through $\text{OH} + \text{C}^+ \rightarrow \text{H} + \text{CO}^+$ followed by $\text{H}_2 + \text{CO}^+ \rightarrow \text{H} + \text{HCO}^+$. However, for our sources, [CII] $158 \mu\text{m}$ data indicate $N(\text{C}^+)/N(\text{CO}) \lesssim 10^{-2}$. Translucent clouds are generally weak in HCO^+ emission (Gredel et al. 1994).

The velocities of the H_3^+ absorptions are consistent with those of the submillimeter emission lines of C^{17}O and C^{34}S , suggesting that the H_3^+ absorbers are in the vicinity of the infrared sources. However, the correlation of $N(\text{H}_3^+)$ with distance remains after subtracting the dense core contribution (Table 2), suggesting a non-local origin. Al-

together, the data indicate that the contribution of the envelopes to $N(\text{H}_3^+)$ varies from $\sim 10^{13}$ to $\sim 10^{14} \text{ cm}^{-2}$, and that any additional absorption seen in sources at $d > 2 \text{ kpc}$ occurs in intervening clouds.

In summary, observations of H_3^+ absorption and H^{13}CO^+ emission lines, combined with models of the temperature and density structure of the sources, constrain the cosmic-ray ionization rate to $\zeta_{\text{CR}} = (2.6 \pm 1.8) \times 10^{-17} \text{ s}^{-1}$, with upper limits that are factors of 3–5 higher. Future tests of the results include more sensitive observations of H_3^+ toward W 3 IRS5 and NGC 2264, velocity-resolved observations to search for H_3^+ absorption at off-set velocities from the dense cores, observations of more distant sources to test the correlation with distance, and observations of HCO^+ infrared absorption lines to directly compare with H_3^+ and CO infrared absorption.

Acknowledgements. We thank Neal Evans, Dan Jaffe, Tom Geballe and John Black for useful discussions. This research is supported by NWO grant 614-41-003.

References

- de Boisanger, C., Helmich, F. P. & van Dishoeck, E. F. 1996, *A&A*, 310, 315
- Dinelli, B. M., Neale, L., Polyansky, O. L. & Tennyson, J. 1997, *J. Mol. Sp.* 181, 142
- Federman, S. R., Weber, J. & Lambert, D. L. 1996, *ApJ*, 463, 181
- Geballe, T. R., McCall, B. J., Hinkle, K. H. & Oka, T. 1999, *ApJ*, 510, 251
- Geballe, T. R. & Oka, T. 1996, *Nature*, 384, 334
- Gredel, R., van Dishoeck, E. F. & Black, J. H. 1994, *A&A*, 285, 300
- Hartquist, T. W., Doyle, H. T. & Dalgarno, A. 1978, *A&A*, 68, 65
- Hollenbach, D. J. & Tielens, A. G. G. M. 1997, *ARA&A*, 35, 179
- Hunter, S. D., Bertsch, D.L., Catelli, J.R. et al. 1997, *ApJ*, 481, 205
- Lee, H.-H., Bettens, R., & Herbst, E. 1996, *A&AS*, 119, 111
- Maloney, P. R., Hollenbach, D. J. & Tielens, A. G. G. M. 1996, *ApJ*, 466, 561
- McCall, B. J., Geballe, T. R., Hinkle, K. H. & Oka, T. 1999, *ApJ*, 522, 338
- Millar, T. J., Farquhar, P. R. A. & Willacy, K. 1997, *A&AS*, 121, 139
- Mitchell, G. F., Lee, S. W., Maillard, J. -P., Matthews, H., Hasegawa, T. I. & Harris, A. I. 1995, *ApJ*, 438, 794
- Mitchell, G. F. & Maillard, J. -P. 1993, *ApJ*, 404, L79
- Mitchell, G. F., Maillard, J.-P., Allen, M., Beer, R., & Belcourt, K. 1990, *ApJ*, 363, 554
- Tielens, A. G. G. M., Tokunaga, A. T., Geballe, T. R. & Baas, F. 1991, *ApJ*, 381, 181
- Timmermann, R., Bertoldi, F., Wright, C. M. et al. 1996, *A&A*, 315, L281
- van der Tak, F. F. S., van Dishoeck, E. F., Evans, N. J., II, Bakker, E. J., & Blake, G. A. 1999, *ApJ*, 522, 991
- van der Tak, F. F. S., van Dishoeck, E. F., Evans, N. J., II, & Blake, G. A. 2000, *ApJ*, 537, 283

- van Dishoeck, E. F. & Black, J. H. 1986, *ApJS*, 62, 109
van Dishoeck, E. F. & Black, J. H. 1989, *ApJ*, 340, 273
Webber, W. R. 1998, *ApJ*, 506, 329